Boron Nitride: Novel ceramic reductant for low-activity waste vitrification.

RIGBY, Jessica, MARCIAL, Jose, POKORNY, Richard, KLOUZEK, Jaroslav, HAN, Kee Sung, WASHTON, Nancy, FERKL, Pavel, HRMA, Pavel, SCRIMSHIRE, Alex <http://orcid.org/0000-0002-6828-3620>, BINGHAM, Paul <http://orcid.org/0000-0001-6017-0798>, HALL, Mark, EATON, Will and KRUGER, Albert

Received: 1 March 2024 | Revised: 4 September 2024 | Accepted: 19 September 2024

DOI: 10.1111/jace.20192

Journal of the American Ceramic Society

RESEARCH ARTICLE

Boron nitride: Novel ceramic reductant for low-activity waste vitrification

Jessica C. Rigby[1] | **José Marcial**[1] | **Richard Pokorny**[2,3] | **Jaroslav Kloužek**[2,3] | **Kee Sung Han**[1] | **Nancy Washton**[1] | **Pavel Ferkl**[1] | **Pavel Hrma**[4] | **Alex Scrimshire**[5] | **Paul A. Bingham**[5] | **Mark Hall**[1] | **Will Eaton**[1] | **Albert A. Kruger**[6]

[1]Pacific Northwest National Laboratory, Richland, Washington, USA

[2]University of Chemistry and Technology Prague, Prague, Czech Republic

[3]Institute of Rock Structure and Mechanics of the Czech Academy of Sciences, Prague, Czech Republic

[4]AttainX, Support Services Contractor to the Office of River Protection, U.S. Department of Energy, Richland, Washington, USA

[5]Materials and Engineering Research Institute, College of Business, Technology and Engineering, Sheffield Hallam University, Sheffield, UK

[6]U.S. Department of Energy, Office of River Protection, Richland, Washington, USA

Correspondence
Jessica C. Rigby
Email: jessica.rigby@pnnl.gov

Funding information
U.S. Department of Energy (DOE) Waste Treatment and Immobilization Plant; Pacific Northwest National Laboratory; Battelle, Grant/Award Number: DE-SAC05-76RL01830; Materials Engineering and Research Institute; Sheffield Hallam University; Czech Ministry of Education, Youth and Sports, Grant/Award Number: LUAUS23062

Abstract

During vitrification of radioactive wastes, excessive foaming reduces processing rates within melters by hindering heat transfer from the molten glass pool to the reacting melter feed. Formulations of low-activity waste (LAW) melter feeds, for vitrification at the Waste Treatment and Immobilization Plant at the Hanford Site, conventionally include the addition of sucrose to mitigate excessive foaming by hastening the denitration process. However, incomplete combustion of sucrose produces organics such as acetonitrile (C_2H_3N) that may exceed bounding limits of downstream effluent treatment facilities. Using boron nitride (BN) as an alternate reductant to sucrose, in a representative LAW melter feed reduced C_2H_3N production by 90% by preventing the low-temperature sucrose–nitrate reactions. Furthermore, foaming was suppressed due to the higher decomposition temperature of BN than H_3BO_3 meaning a delayed reaction of a large fraction of boron with the transient glass-forming melt until above the foam onset temperature, thus reducing the quantity and viscosity of the connected melt and trapping less gas in the foam layer.

KEYWORDS
alternate reductants, off-gas, radioactive waste, redox, vitrification

1 | INTRODUCTION

Sucrose is the baseline reductant for the vitrification of Hanford low-activity waste (LAW) at the Waste Treatment and Immobilization Plant (WTP).[1–7] Sucrose addition to the mixture of LAW and glass forming and modifying additives (GFMAs) results in a reduction of foaming behavior and higher production rates for a variety of high-nitrate feed simulants.[8–12] Sucrose reduces the primary foam during feed-to-glass conversion by reacting with nitrates at low temperatures (200°C–600°C), so fewer evolved gases are trapped beneath a viscous connecting melt at higher temperatures (>600°C).[9,10] The nominal molar quantity of sucrose is scaled such that the atomic ratios of organic carbon from the waste organics and sucrose to nitrogen from nitrates and nitrites is equal to 0.75.[10,12,15,16] This C/N ratio was found optimal in the compositional range tested for SO_3 retention, iron redox state (avoiding over-reduction of the melt), and sufficient foam reduction.[10,12,15,16]

The sucrose/nitrate reaction that aids in reducing the foam volume also produces acetonitrile (C_2H_3N) in the off-gas system.[17–19] Experimental work using research-scale systems, that resemble the direct-feed LAW (DFLAW) flowsheet, has shown that most of the acetonitrile will partition in the evaporator condensate, which is directed to the Hanford Effluent Treatment Facility (ETF).[19] The acetonitrile concentration in these effluents was determined to be unsuitable for processing in the ETF exceeding waste acceptance criteria.[20,21] Since this was reported, costly downstream modifications to the treatment flowsheet have been adopted for treatment of the acetonitrile in the ETF, including a steam stripper.[20–22] No promising solutions have yet been proposed upstream of the ETF that would allow flexibility in plant operations and provide less costly options for future operations.

Estimates of acetonitrile present in the primary off-gas system are around 1 g kg^{-1} of sugar, or 2 g kg^{-1} of organic carbon equivalent added to the melter feed.[19] Uncertainties remain where high contents of other organics and water are present in the feed.[23] Alternate carbon-based reductants, such as formic acid, have been explored for the WTP and employed at other vitrification plants.[8,24–27] Other carbon-based reductants are not immune from causing concerns in the off-gas system, as many carbon forms will form products of incomplete combustion in the off-gas system. Furthermore, formic acid recently caused apprehensions over the production of flammable levels of hydrogen, propelling exploration of alternatives.[24,28,29] Ceramic, or other inorganic reductants, as an alternative to organic reductants, would alleviate many of these concerns, removing the source of added carbon for acetonitrile generation.

Boron nitride (BN) ceramic powder provides an isostructural and isoelectronic compound to carbon.[30] Hexagonal BN, h-BN, has a melting temperature of around 3000°C,[31] and in h-BN nanoplatelets, a stable mass has been observed up to 1000°C and then the oxidation reaction proceeds.[32]

$$2\,BN + 3/2\,O_2 \rightarrow B_2O_3 + N_2 \quad (1)$$

To the authors' knowledge, BN has not been added to waste feeds as a reductant, nor were we able to identify any literature pertaining to its addition to any glass-forming melt.

This study endeavors to investigate the potential benefits of BN as a reducing agent in a simulated DFLAW feed and initiate the exploration of BN and other ceramic reductants across waste treatment programs and potentially also into the commercial glass manufacturing industry. By studying the foaming properties and gas evolution in a representative DFLAW melter feed with sucrose compared to alternatives batched with varying ratios of BN, the following study will evaluate the effectiveness of BN as a foam-reducing agent and in suppression of acetonitrile evolution. By structural investigation of heat-treated feed samples, the work intends to reveal some of the governing chemistry behind differences in foaming and gas evolution and determine the effect on the glass redox state.

2 | MATERIALS AND METHODS

The 241-AP-107-simulated tank waste feed, herein described as AP-107, was batched as described in Table 1. The GFMAs were batched as described in Table 2, where the nominal AP-107 composition, containing sucrose for the purpose of reducing foam, is based on the "AP107WDFL" formulation.[33] From this baseline composition, the other compositions were designed where BN was substituted for C in sucrose in an equimolar ratio. For the feeds with BN added, H_3BO_3 was reduced to account for the excess B to ensure that the final glass composition was consistent. The bounding case for "maximum" amount of BN addition was a feed in which BN entirely replaced the H_3BO_3 added as a GFMA, which resulted in a "BN/N" ratio of 1.75.

For simplicity, the nomenclature used for BN-bearing melter feeds in this study is BN*Y*, where *Y* is the BN/N molar ratio. Feeds with BN/N molar ratios of 1.75, 0.75, 0.50, and 0.25 were formulated. The raw materials for the simulated waste feeds and GFMAs were batched in deionized water and then thoroughly mixed, before drying for at least 24 h at 105°C. Once dry, feeds were

TABLE 1 Nominal composition of the AP-107 simulated waste feed.[33]

Simulated waste constituents	Mass added to feed to make 100 g of glass (g/100 g glass)
Re solution (769 mg L^{-1})	1.05
$Al(NO_3)_3 \cdot 9H_2O$	13.58
$Ca(NO_3)_2 \cdot 4H_2O$	0.03
Na_2CrO_4	0.16
$Fe(NO_3)_3 \cdot 9H_2O$	0.02
KOH	0.46
NaOH	8.61
$Ni(OH)_2$	0.004
PbO	0.002
SiO_2	0.007
NaCl	0.69
NaF	0.09
$Na_3PO_4 \cdot 12H_2O$	0.69
Na_2SO_4	0.78
$NaNO_2$	7.70
$NaNO_3$	7.02
Na_2CO_3	5.70
$NaC_2H_3O_2$	0.57
$NaCHO_2$	0.37
$Na_2C_2O_4$	0.10

crushed to a fine powder using a tungsten carbide puck mill.

For each composition variation, the foam volume profile during melting was measured using a feed volume expansion test (FET) as described by Hilliard and Hrma,[34] and Marcial et al.[35] Approximately 0.9 g of dried feed was pressed into 13-mm diameter pellets under 7 MPa pressure for three intervals of 30 s. The pellets were loaded into a furnace with a viewport and heated from room temperature at 10°C min^{-1}. Images were taken every 10°C, and the FET trial was deemed complete once the pellet had physically melted to a flat pool, between 1000°C and 1150°C. The volume, V, was estimated assuming rotational symmetry around a vertical axis and then normalized to the volume of the final glass melt, by the following equation:

$$V_G = \left(m_{\text{feed}}/\rho_{\text{glass}}\right)\ (1 - L_I) \quad (2)$$

where m_{feed} is the mass of the feed added to form the pellet, ρ_{glass} is the density of the glass (estimated to be 2.5 g cm^{-3}), and L_I is the loss on ignition. FET experiments were performed in duplicate or triplicate for error analysis.

For evolved gas analysis, approximately 1 g of each powdered feed was loaded into a silica test tube with a gas inlet and outlet secured to the top and placed in an electric furnace. The feeds were heated to 1150°C at a rate of 10°C min^{-1}, while a Hiden Analytical HPR R&D20 evolved gas analysis monitored the signals of the mass-to-charge (m/z) values, defined in Table S1, evolving from the test tube. Argon carrier gas at a flow rate of 50 mL min^{-1} created an inert atmosphere to prevent overlap with gas evolving from the feed, particularly O_2 and N_2. The measured intensities of the m/z signals were normalized to the intensity of the carrier gas to convert into parts per million (ppm) values. The inert atmosphere could overestimate the total quantity of gases evolved compared to the air atmosphere that the feed would experience in the furnace; however, the comparison of the different feeds in a controlled atmosphere is of interest to this study. Background measurements were taken for approximately 5 min for each feed before beginning the temperature ramp; the background gas quantities were subtracted from the collected quantities of gases evolving during heating.

Ten-gram samples of each feed were heated to temperatures representative of key stages of foaming based on the FET results; these temperatures were 105°C, 400°C, 700°C, 1000°C, and 1150°C. The feeds were quenched in air once they had reached the desired temperature to provide a snapshot of the chemical nature of the feed at that stage of melting. The samples were then milled and analyzed for composition by electron probe microanalysis (EPMA)/wavelength dispersive spectroscopy, and images of phase distribution are shown in Figures S1-S4 in the Supporting Information. Phase identification and quantification were performed by X-ray diffraction (XRD), and analysis of boron speciation by ^{11}B magic angle spinning nuclear magnetic resonance (NMR).

Elemental mapping was performed using a JEOL 8530F EPMA field emission gun electron microscope outfitted with wavelength dispersive spectrometers operated at 15 keV and 50 nA. Heat-treated and -dried feed powders were prepared for EPMA by mounting in epoxy resin. Following mounting in epoxy, samples were polished using 200, 400, 600, 800, and 1200 grit silicon carbide (SiC) grinding paper with a mineral oil lubricant. A mineral oil lubricant was used instead of water because some species were water soluble. The polished surfaces were cleaned with ethanol. To reduce charging during EPMA, samples were sputter coated with a 2-nm iridium coating. Elemental maps were taken for Na, Ca, Al, Fe, B, N, and Si.

XRD was performed in the range of 5°–70° 2θ on a Bruker D8 Advance X-ray diffractometer with a Cu Kα X-ray tube. A step size of 0.015° 2θ and dwell time of 1.5 s per step was used for these measurements. Prior to measuring, a 5 wt% spike of CeO_2 internal standard was added to each XRD sample before crushing in a tungsten-carbide puck mill. The amorphous fraction was calculated using

TABLE 2 Nominal composition of the AP-107 glass forming and modifying additives (GFMAs) for each variation in sucrose and boron nitride content.

	Mass added to feed to make 100 g of glass (g/100 g glass)					
Glass-forming chemicals	**Nominal AP-107 C/N = 0.75**	**AP-107 No sucrose C/N = 0.06**	**BN0.75 BN/N = 0.75**	**BN0.50 BN/N = 0.50**	**BN0.25 BN/N = 0.25**	**BN1.75 BN/N = 1.75**
Al_2SiO_5	6.93	6.93	6.93	6.93	6.93	6.93
H_3BO_3	17.72	17.72	10.12	12.65	15.18	0.0
$CaSiO_3$	8.62	8.62	8.62	8.62	8.62	8.62
Fe_2O_3	5.29	5.29	5.29	5.29	5.29	5.29
Li_2CO_3	2.22	2.22	2.22	2.22	2.22	2.22
Mg_2SiO_4	2.96	2.96	2.96	2.96	2.96	2.96
SiO_2	35.77	35.77	35.77	35.77	35.77	35.77
TiO_2	1.48	1.48	1.48	1.48	1.48	1.48
ZnO	3.49	3.49	3.49	3.49	3.49	3.49
$ZrSiO_4$	4.54	4.54	4.54	4.54	4.54	4.54
$C_{12}H_{22}O_{11}$	5.97					
BN			3.03	2.02	1.01	7.08
Total	141.57	136.65	131.03	132.55	134.08	124.95

the internal standard method and Rietveld refinement in Topas software.

The ^{11}B direct polarization experiments were performed using a 20 Tesla wide bore Varian Nuclear Magnetic Resonance spectrometer, operated with a 4.0-mm triple resonance probe tuned to a ^{11}B frequency of 272.631 MHz. Spectral acquisition was performed by collecting 4096 transients using calibrated ^{11}B $\pi/20$ pulses of 0.4 μs, a 625 kHz sweep width, a spinning speed of 15 kHz, and a 2.0 s recycle delay. The time domain–free induction decays were apodized using exponential functions corresponding to 150 Hz of Lorentzian broadening followed by a Fourier transformation. The 0 ppm reference of ^{11}B resonances was defined using $BF_3O(CH_2CH_3)_2$ and 0.5 M H_3BO_3 as a secondary reference at 19.6 ppm. Ratios of BO_3:BO_4:BN_3 were calculated using resonance line fittings conducted in the Nuts software environment (Acorn NMR, Inc.). The primary uncertainty in the reported values for BO_3:BO_4:BN_3 ratios arises from spectral noise, which is diminished by collecting many transients for each spectrum. The standard deviation in the BO_3:BO_4:BN_3 ratios was estimated with a Monte Carlo algorithm in the Mathematica programming environment (Wolfram) using the root-mean-square deviation of a sample of random spectral noise.[36,37] For all BO_3:BO_4:BN_3 ratio values reported here, the error is ±0.5% or lower.

The ^{57}Fe Mössbauer spectroscopy was employed to determine the iron redox state of the final glasses. Samples heat treated to 1150°C were powdered, diluted with graphite, and inserted into the room temperature spectrometer. Decay of a 25 mCi ^{57}Co source in a Rh matrix produced 14.4 keV γ-rays to be absorbed by the sample. The source oscillated at a constant acceleration by a SeeCo W304 drive unit, and the γ-rays were detected by a SeeCo 45431 Kr proportional counter operating with 1.745 kV bias voltage applied to the cathode. Spectra of the photons transmitted through the sample were collected over the velocity range ±12 mm s^{-1} and were calibrated relative to α-Fe.[37] Recoil software was used to fit pseudo-Voight doublets to the collected spectra, and the iron redox state was determined by the ratio of the peak areas of Fe^{3+} and Fe^{2+} sites, assuming a recoil-free fraction ratio of $f(Fe^{3+}/Fe^{2+}) = 1.0$.[39]

3 | RESULTS AND DISCUSSION

3.1 | Slurry properties

A white film rose to the surface of the slurry feed after BN was added, as shown in Figure 1, likely due to the low density of the BN particles. The feed required mixing at 15-min intervals during the first 3 h of the drying period. Milling then ensured a homogenous distribution of the BN throughout the powdered feed. WTP LAW design involves continuous mixing of the waste feed and GFMAs before entry to the melter.[2] Inhomogeneity of the feed slurry would require consideration where continuous stirring of the feed slurry is not a practical option.

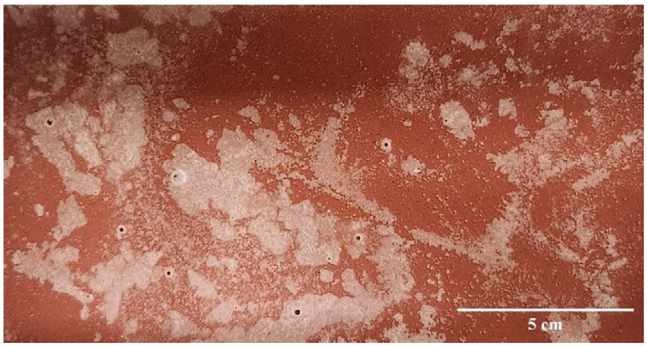

FIGURE 1 Segregation of the boron nitride (BN) powder from the rest of the AP-107 BN0.75 mixed slurry feed.

3.2 | Foaming and gas evolution

A comparison of major evolving gases, CO, NO, O_2, CO_2, and NO_2, and the feed volume expansion with temperature, is shown in Figure 2 for each of the feeds. Maximum feed volume during FETs of AP-107 with no reducing agent is 18× the volume of glass produced ($V/V_G = 18$). The addition of sucrose, Figure 2B, reduced the maximum foam volume by around 18% ($V/V_G = 15$). Replacing all H_3BO_3 with BN (BN1.75), Figure 2C, delayed the foam onset to above 1000°C and reduced the maximum foam volume by approximately 77%. For BN0.25, BN0.5, and BN0.75 feeds, the maximum foam volume was reduced by approximately 52%, 72%, and 81%, respectively. Two foaming maxima are distinct in BN0.75 and to a lesser extent in BN0.5 and BN0.25.

The effect of a higher-temperature foaming pattern on the feed processing in electric melters is not clear. This could mean a thinner cold cap with less overall foam, and therefore increased heat transfer to the reacting feed. Alternatively, foam that collapses at higher temperature could restrict heat transfer directly from the melt to the bottom of the cold cap, thus decreasing the melting rate.

Without sucrose addition, in Figure 2A, the majority of the NO evolution overlaps with the onset of foaming, yielding the high peak foam volume. With sucrose addition, Figure 2B, a substantial fraction of the NO is evolved at temperatures as low as 250°C, decreasing the gas produced in the temperature interval of foaming.

For BN0.75, 0.50, and 0.25, in Figure 2D–F, the amount of NO and NO_2 evolving between 600°C and 800°C is similar to the feed without sucrose, contributing to the primary foam peak, and suggesting that unlike sucrose, BN does not react chemically with the nitrogen species in the feed. The quantity of gases in the primary foam region, 700°C–900°C, is greater in the BN-containing feeds than the nominal and no sucrose AP-107 feeds, but the foam volume is less. The mechanism of foam reduction using sucrose as a reductant is chemical, involving the partial destruction of nitrates at low temperatures, prior to the foam onset.[40] These results suggest that foam reduction using BN is related to the quantity and/or viscosity of the transient melt forming around the gasses and trapping them as foam. This reasoning is explored in the following section on the structure of the material with temperature.[35,41–43]

The secondary peak in the BN-containing feeds may be caused by the small N_2 evolution above 900°C with lesser contribution from SO_3 evolution (Figure 3A). N_2 evolution above 1000°C is in keeping with the decomposition of BN with temperature from reaction (1) discussed in Section 1.[32] The temperature onset of SO_2 evolution decreases with increasing BN content. The amount of SO_3 released is significantly greater in the BN0.75 feed than the other BN-containing feeds, while nominal AP-107 does not evolve SO_2 in the temperature region measured. The retention of SO_3 in the glass will be of interest to waste processing and therefore should be investigated further.

With the removal of sucrose, and replacement with BN, there is a reduction of over 90% of the acetonitrile produced by the feed during melting, shown in Figure 3B.

3.3 | Structure and phase composition

For heat-treated AP-107, BN0.25, BN0.50, and BN0.75 at 105°C, 400°C, 700°C, 1000°C, and 1150°C, proportions of crystalline phases were determined by refinement of collected XRD patterns, given in Figures S5 to S29 in the Supporting Information; these allowed for quantification of the amorphous phase at each of the temperatures shown in Figure 4.

Figure 4E takes the quantity of crystalline phase and mass loss during melting to approximate the proportion of amorphous phase at each temperature. The difference in the quantity of amorphous phase is significant at 700°C, where a higher proportion of silica has dissolved into the transient melt in AP-107 than in any of the BN feeds. This would mean the transient melt forming around the other constituents and trapping gases from gas-evolving reactions would be much more viscous in the AP-107 feed than the BN-added feeds.

The evolution of the structure of boron, investigated by ^{11}B NMR, is displayed in Figure 5. BN can be ascribed to a signal centered near 26 ppm consistent with previously published chemical shifts for BN_3.[44,45] Additional signals observed correspond to BO_3 (~15 ppm) and BO_4 (~0 ppm) consistent with previously published chemical shifts with aluminosilicate glasses.[36,46] The doublet observed for BN_3 and BO_3 signals is not due to multiple crystallographic special sites but instead to the quadrupolar line splitting.[44]

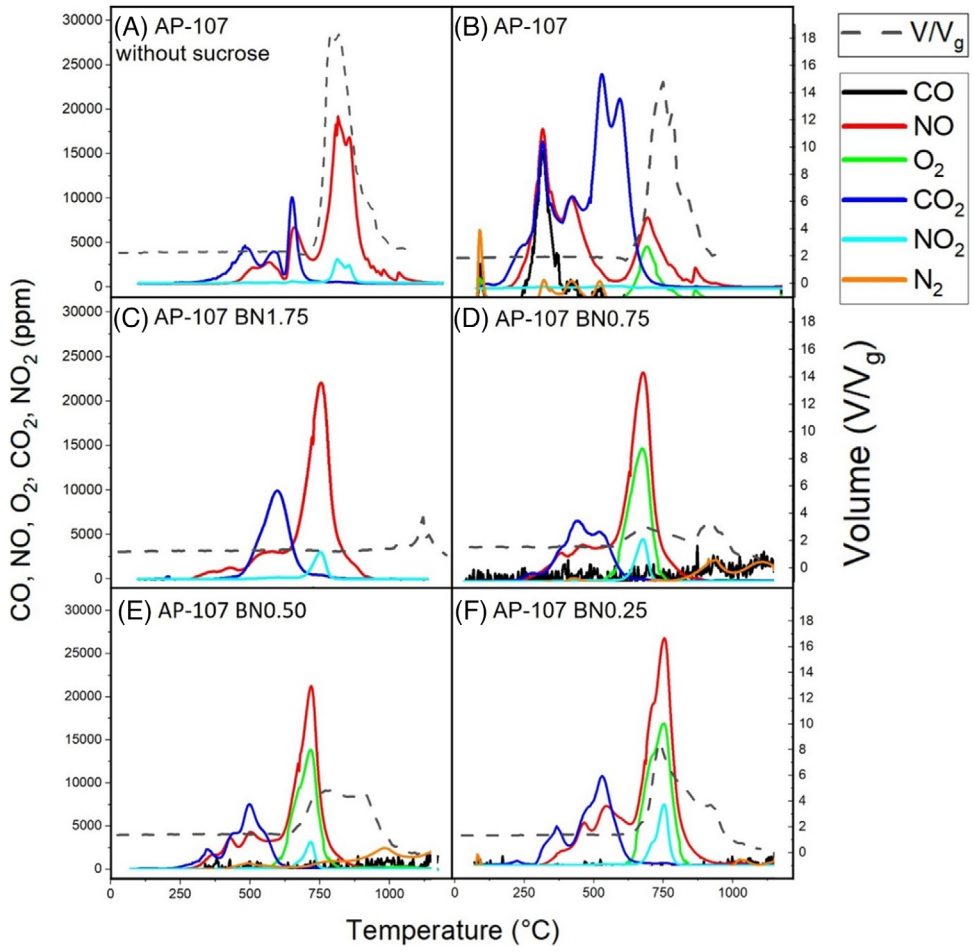

FIGURE 2 Normalized volumetric expansion and evolution of CO, CO_2, N_2, NO, NO_2, and O_2 gases from AP-107 batched (A) without sucrose, (B) with sucrose at C/N 0.75, (C) batched with boron nitride equivalent BN/N of 1.75, (D) 0.75, (E) 0.50, and (F) 0.25.

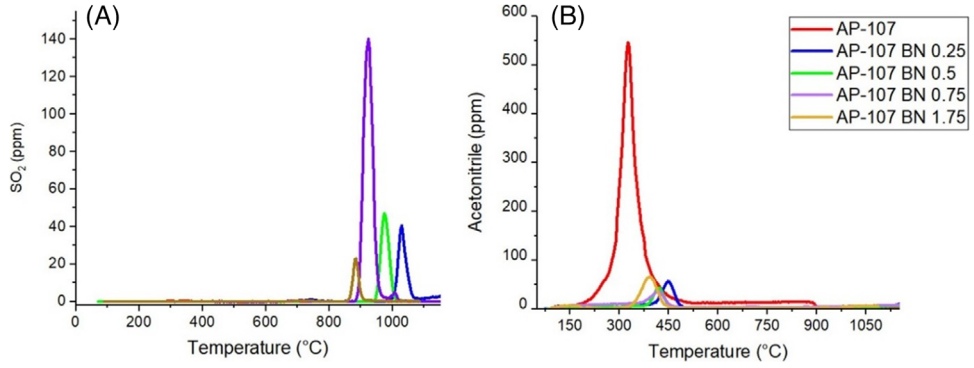

FIGURE 3 (A) SO_2 and (B) acetonitrile evolution nominal AP-107 BN at equivalent BN0.25, 0.50, 0.75, and 1.75.

The nominal AP-107 feed, shown in Figure 5A, follows a transition from sharp to broadened features with increasing temperature, without a chemical shift indicating a transition from highly structured crystalline to amorphous BO_3 and BO_4. The relative abundance of BO_3 increases with temperature (Figure 6). For BN0.75, there is a non-linear relative increase in BN_3 phase proportion from 105°C to 700°C. The BO_4 signal is consistent throughout the temperature range, and the proportion of BO_3 changes relatively with the proportion of BN_3. At 1150°C, there is no discernable BN and instead BN has oxidized to either BO_3 or BO_4.

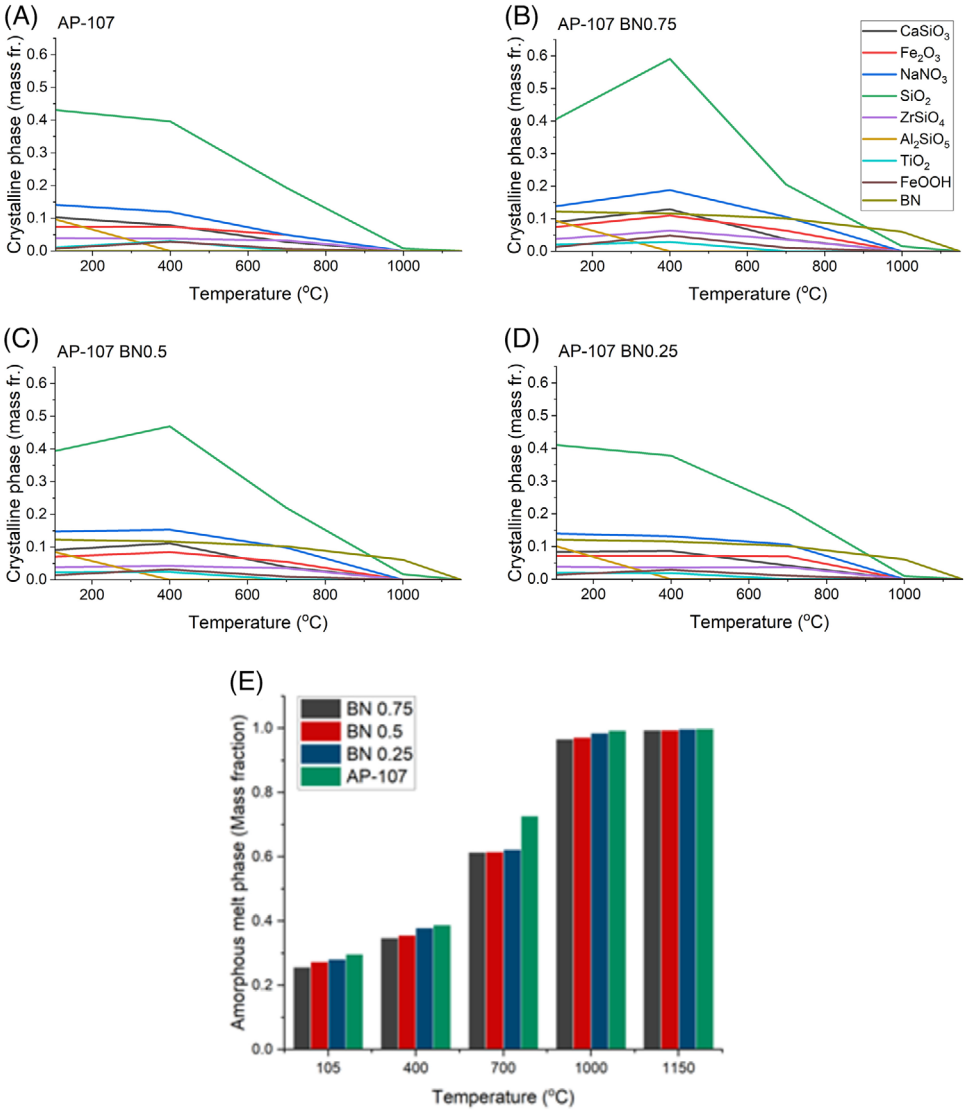

FIGURE 4 Mass fraction of crystalline phases in the feed at 105°C, 400°C, 700°C, 1000°C, and 1150°C for AP-107 with sucrose and with varying BN content by refinement of X-ray diffraction (XRD) patterns and fraction of amorphous phase in the feeds with sucrose and BN at 105°C, 400°C, 700°C, 1000°C, and 1150°C.

The ^{10}B isotopic enrichment, using $H_3{}^{10}BO_3$-containing BN0.75 melter feed, was performed to directly observe only the evolution of the arrangement of boron from BN during heating. In the ^{10}B-enriched feed, Figure 5C, BN remains undissolved until 1000°C after which the B oxidizes primarily to BO_3 at 1000°C, while minor quantities of BO_4 emerge at 1150°C. ^{11}B NMR data of AP-107 1.75BN, where BN is the only boron raw material, in Figure 5D, suggest that BN begins dissolving as temperatures approach 1000°C. The BN 1.75 sample data mirrors that of the ^{10}B-enriched feed, in all but having a greater relative proportion of BO_4 structural units.

The decomposition of BN observed by ^{11}B NMR, Figure 6, shows no interaction of BN with other feed components until above the foam onset temperature found in the feed expansion curve in Figure 2 to be >700°C. With boron being a key component of the low-temperature transient glass forming melt in AP-107, this is the origin of the lack of amorphous phase fraction in the BN-containing feeds. Since both less silica and boron are dissolved into the transient melt, the melt readily collapses causing lower overall foam volume despite large quantities of gases evolving. Both the quantity and viscosity of transient melt are reduced compared to the nominal feed containing sucrose at 700°C where the major gas evolution occurs.

Once the boron from BN starts to react with the transient melt, the rate of silica dissolution increases in the BN0.25, 0.50, and 0.75, Figure 4, such that they match the fraction in the nominal AP-107 feed by 1000°C. This will increase

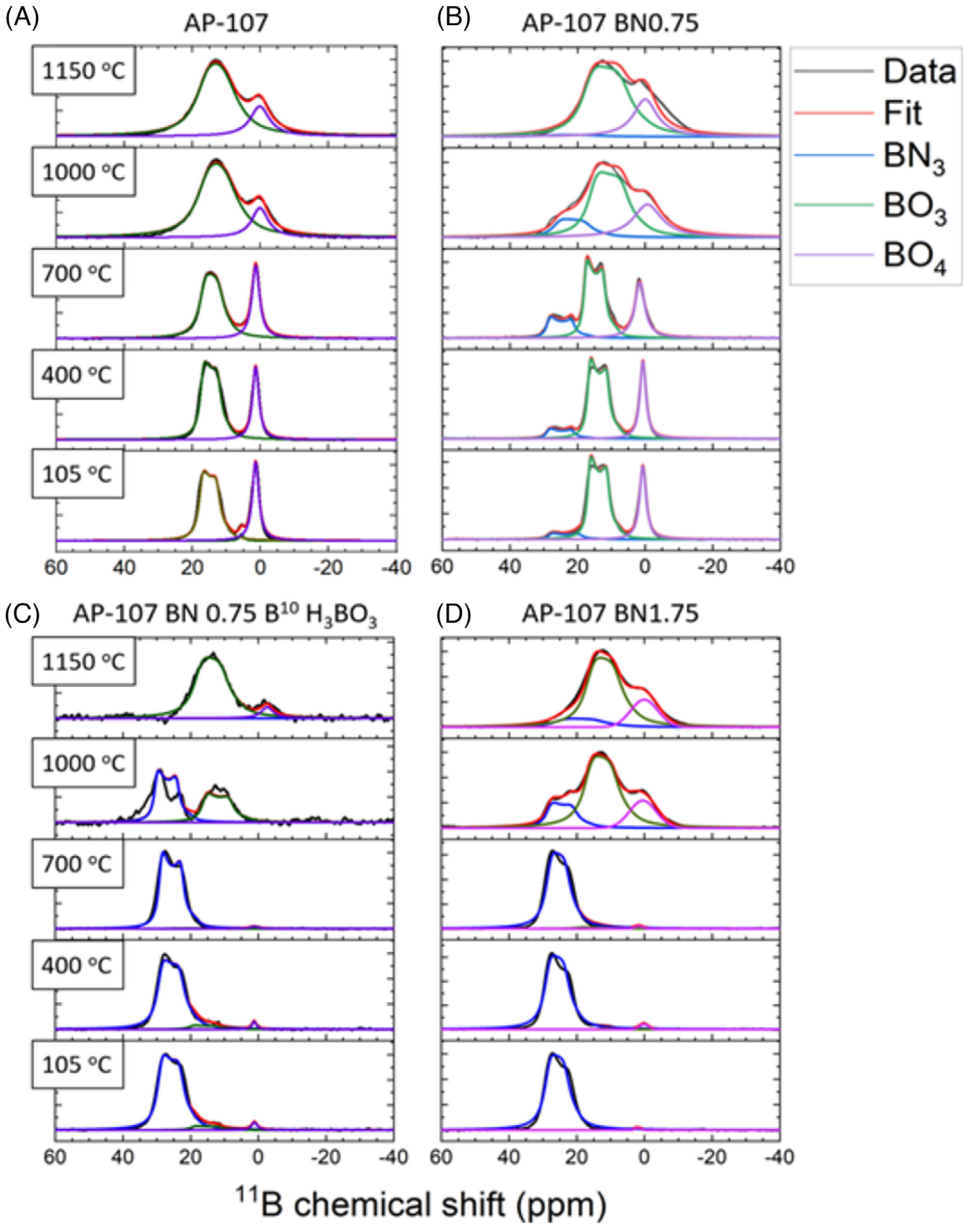

FIGURE 5 Evolution of boron structure with temperature by ^{11}B NMR of (A) the AP-107 feed, (B) the BN0.75 feed, (C) an AP-107 feed batched with isotopic ^{10}B H_3BO_3 aiming to isolate the BN behavior with temperature, and (D) the BN1.75 feed.

the viscosity of the glass-forming melt and begin trapping more gases, causing the secondary foam peak observed, predominantly in the higher BN feeds (Figure 2). The oxidation reaction (1) of BN postulated to explain the N_2 gas evolution peak >1000°C in Section 3.2, from the literature in Section 1, is also supported by the BN decomposition in Figures 5 and 6.

3.4 | Iron redox

Hyperfine fitting parameters of the pseudo-Voight functions fitted to the ^{57}Fe Mössbauer data in Figure 7 are detailed in Table 3 along with the iron redox state of each sample based on the relative intensities of the Fe^{3+} and Fe^{2+} features identified from the spectra.[47]

For the nominal AP-107 feed, only a single Fe^{3+} doublet is resolved. With increasing BN content, the proportion of iron in Fe^{2+} sites increases, beginning at an abundance of 24% ± 2% in the BN0.25 sample and reaching 55% ± 2% for the BN0.75 sample, making the redox state of Fe in the BN0.75 sample (Fe^{3+}/Fe_T) approximately 0.45. Where Fe^{2+} phases are present, only one Fe^{3+} site is resolvable. In all three samples, the Fe^{3+} site is tetrahedral on average. There are no magnetic phases resolved in either of the spectra.[48]

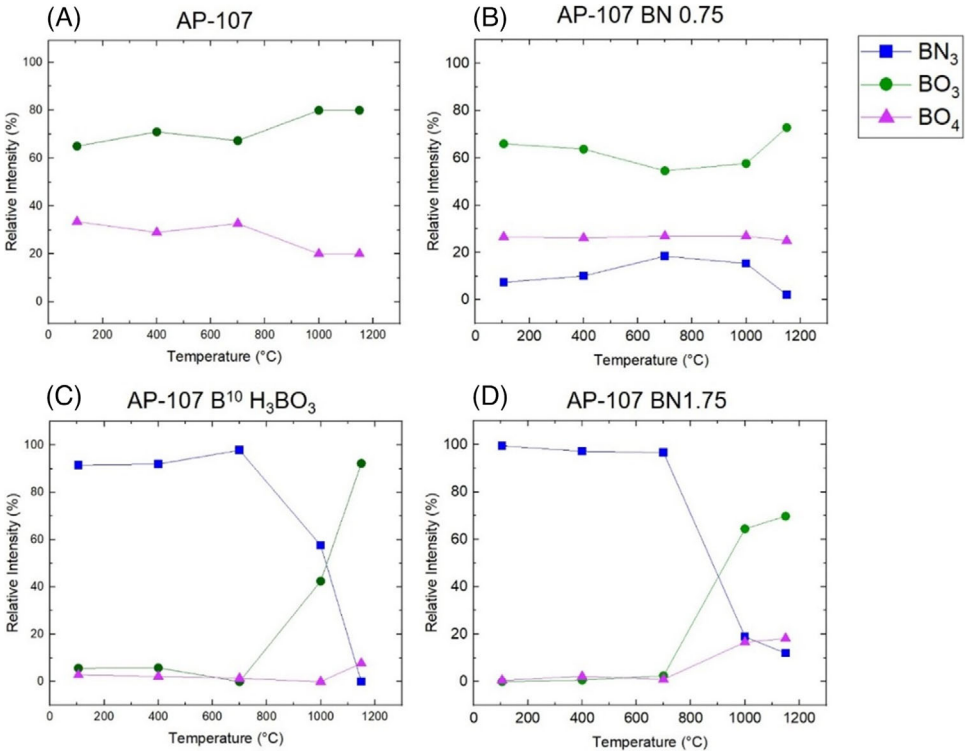

FIGURE 6 Proportion of ^{11}B as BN_3, BO_3, and BO_4 structures by ^{11}B NMR for (A) the nominal AP-107 feed, (B) the BN0.75 feed, (C) a BN0.75 feed batched with isotopic ^{10}B H_3BO_3 aiming to isolate the BN behavior with temperature, and (D) the BN1.75 feed.

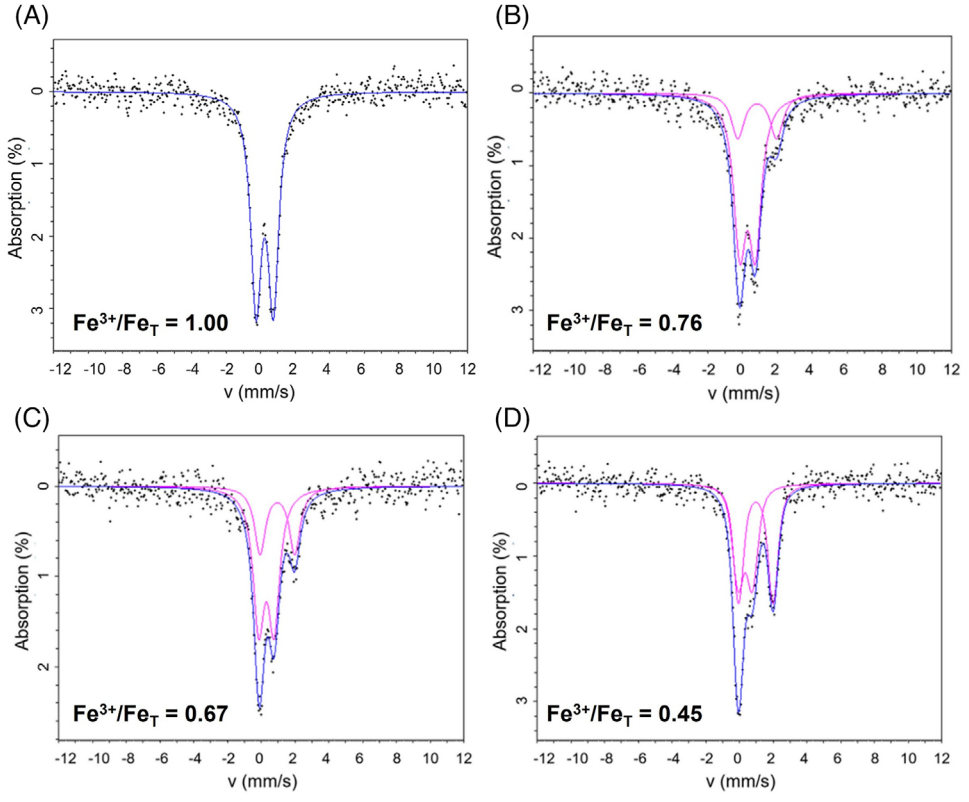

FIGURE 7 *x*-VBF of the ^{57}Fe Mössbauer spectra of (A) the nominal AP-107 1150°C sample, (B) the BN0.25 1150°C sample, (C) the BN0.50 1150°C sample, and (D) the BN0.75 1150°C sample.

TABLE 3 Hyperfine splitting parameters from pseudo-Voight fits of ^{57}Fe Mössbauer spectra collected for AP-107 and BN0.75 glasses.

Sample	Site	CS mm s^{-1}	QS mm s^{-1}	Relative abundance %	SIron redox Fe^{3+}/Fe_T
AP-107	^{IV} Fe^{3+}	0.23	0.87	30	1.00
	^{VI} Fe^{3+}	0.26	1.08	70	
BN0.25	$^{(IV/VI)}$ Fe^{3+}	0.30	0.89	76	0.76
	$^{VI}Fe^{2+}$	0.68	2.23	24	
BN0.50	$^{(IV/VI)}$ Fe^{3+}	0.31	0.91	67	0.67
	$^{VI}Fe^{2+}$	0.96	2.05	33	
BN0.75	$^{(IV/VI)}$ Fe^{3+}	0.34	0.86	45	0.45
	$^{VI}Fe^{2+}$	0.99	2.01	55	

CS, centre shift relative to α-Fe, ±0.02 mm s^{-1} relative abundance ±2%, QS, quadrub

The reduction of iron from Fe^{3+} to Fe^{2+} correlates with the BN content. Over reducing the melt can lead to undesirable phenomena, such as the precipitation of metallic phases and sulfides.[26,49] Fe^{2+}/Fe^{3+} ratios between 0.09 and 0.33 are suggested for processing of nuclear waste to "provide sufficient safety against foaming or precipitation."[49,50] The heavily reduced iron in the BN-containing feeds exposes the insufficiency in assuming an equivalent reducing power between BN and the C in sucrose. Perhaps the use of a more robust stoichiometric calculation for BN addition would be suitable for implementation in this case.[23] Additional discussion on this is provided in the Supporting Information.

4 | CONCLUSION

Employing BN as a replacement for sucrose as an alternate reductant in the LAW waste feed studied reduced 90% of the acetonitrile produced during melting. If implemented in the WTP, this could alleviate strain on secondary liquid effluent waste processing.

In replacing the sucrose, a proportion of the glass-forming additive H_3BO_3 was also removed to account for the B in BN. The higher-temperature incorporation of boron in the transient glass-forming melt caused by this replacement is the mechanism that leads to a reduction in foaming. Representative melter testing and observation of the cold cap would be required to understand how such foaming behavior influences the processing rates of the feeds in a melter. Based on the mechanism of foam control, similar results could be achieved with other ceramic compounds with decomposition temperatures high enough to withhold glass forming species from the low-temperature transient melt, such as B_4C, SiC, and B_6Si.

While a comprehensive study of all impacts of a change of reductant to the WTP processing flowsheet and glass product quality is beyond the scope of the present paper, demonstration of foam control and redox manipulation using ceramic compounds provides potential avenues for exploration that could enhance operational flexibility at the WTP as well as other glass melting processes, and further optimizing the BN addition, for example, adding less than BN/N = 0.25, for desired glass properties while examining whether foam control is still achieved.

ACKNOWLEDGMENTS

The authors gratefully acknowledge financial support from the U.S. Department of Energy (DOE) Waste Treatment and Immobilization Plant Project. Pacific Northwest National Laboratory is operated by Battelle for DOE under contract DE-SAC05-76RL01830. A portion of the research was performed using the Mössbauer capabilities at the Materials Engineering and Research Institute at Sheffield Hallam University. Richard Pokorny acknowledges the financial support from the Czech Ministry of Education, Youth and Sports Project No. LUAUS23062.

ORCID

José Marcial https://orcid.org/0000-0001-6156-5310
Richard Pokorny https://orcid.org/0000-0002-9023-0381
Jaroslav Kloužek https://orcid.org/0000-0002-6826-1632
Pavel Ferkl https://orcid.org/0000-0003-2844-3199
Paul A. Bingham https://orcid.org/0000-0001-6017-0798

REFERENCES

1. Larson DE, Watrous RA, Kruger OL, Nelson JL, Fort LA, Bates SO, et al. Hanford waste vitrification plant technical manual. Richland, WA: Pacific Northwest National Laboratory; 1996. https://doi.org/10.2172/212483
2. Kim DS, Kruger AA, Vienna JD. Preliminary ILAW formulation algorithm description, 24590 LAW RPT-RT-04-0003, Rev. 1. Richland, WA: Office of River Protection; 2012. https://doi.org/10.2172/1110191

3. Matlack KS, Muller IS, Callow RA, D'Angelo N, Bardekci T, Joseph I, et al. Improving technetium retention in Hanford LAW glass—phase 2. (VSL-11R2260-1). Washington, DC: Vitreous State Laboratory, Catholic University of America; 2011. https://doi.org/10.2172/1458754
4. Darling DB, Lee KP, Swanberg DJ, Cree LH. Department of energy responses to the nuclear regulatory commission request for additional information on the draft waste incidental to reprocessing evaluation for vitrification of low activity waste. Richland, WA: Office of River Protection; 2021.
5. Goel A, McCloy JS, Pokorny R, Kruger AA. Challenges with vitrification of Hanford high-level waste (HLW) to borosilicate glass—an overview. J Non-Cryst Solids X. 2019;4:100033. https://doi.org/10.1016/j.nocx.2019.100033
6. Marcial J, Riley BJ, Kruger AA, Lonergan CE, Vienna JD. Hanford low-activity waste vitrification: a review. J Hazard Mater. 2023;461:4–10. https://doi.org/10.1016/j.jhazmat.2023.132437
7. Vienna JD. Nuclear waste vitrification in the United States: recent developments and future options: nuclear waste vitrification in the United States. Int J Appl Glass Sci. 2010;1(3):309–21. https://doi.org/10.1111/j.2041-1294.2010.00023.x
8. Bickford DF, Hrma P, Bowan BW. Control of radioactive waste glass melters: II, residence time and melt rate limitations. J Am Ceram Soc 1990;73(10):2903–15. https://doi.org/10.1111/j.1151-2916.1990.tb06693.x
9. Bunnell LR. Laboratory work in support of West Valley glass development (PNL-6539; Nuclear Waste Treatment Program). Richland, WA: Pacific Northwest National Laboratory; 1988. https://doi.org/10.2172/5196678
10. Matlack KS, Gong W, Muller IS, Joseph I, Pegg IL. Final report—LAW envelope C glass formulation testing to increase waste loading, VSL-05R5900-1 (ORP-56323 Rev 0, 1109496). Washington, DC: Vitreous State Laboratory, The Catholic University of America; 2013. https://doi.org/10.2172/1109496
11. Matlack KS, Muller IS, Gong W, Pegg IL. Final report—DuraMelter 100 tests to support LAW glass formulation correlation development, VSL-06R6480-1, Rev. 0 (ORP-56324/VSL-06R6480-1). Washington, DC: Vitreous State Laboratory, The Catholic University of America; 2006. https://doi.org/10.2172/1109494
12. Matlack KS, Perez-Cardenas F, Pegg IL, Macedo PB, Buechele AC, Hojaji H, et al. Melter Tests with LAW Envelope A and C Simulants to Support Enhanced Sulfate Isncorporation (ORP-63503/VSL-01R3501-2). Washington, DC: Vitreous State Laboratory, The Catholic University of America; 2001.
13. Hrma P, Schweiger MJ, Humrickhouse CJ, Moody JA, Tate RM, Rainsdon TT, et al. Effect of glass-batch makeup on the melting process. Ceramics-Silikaty. 2010;54(3):193–211.
14. Lee S, Jin T, Rivers E, Kloužek J, Luksic S, Marcial J, et al. Effect of sucrose on technetium and rhenium retention during vitrification of low-activity wastes. J Am Ceram Soc. 2022;105(12):7321–33. https://doi.org/10.1111/jace.18701
15. Matlack KS, McKeown D, Hojaji H, Muller IS, Morgan SP, Buechele AC, et al. Melter tests with LAW envelope B simulants to support enhanced sulfate incorporation (Final Report) (ORP-63502/VSL-00R3501-1, Rev.0). Washington, DC: Vitreous State Laboratory, The Catholic University of America; 2000.
16. Matlack KS, Pegg IL, Gong W. Final report: compositional variation tests on DuraMelter 100 with LAW sub-envelope A3 feed in support of the LAW Pilot Melter (ORP-63485/VSL-01R62N0-1 Rev. 2). Washington, DC: Vitreous State Laboratory, The Catholic University of America; 2003.
17. Matlack K, Pegg I. Compilation of off-gas vapor and liquid phase organic information from scale melter testing of LAW simulants (VSL-17S4450-1, Rev A) (ORP-67602-00/VSL-17L4450-1). Washington, DC: Vitreous State Laboratory, The Catholic University of America; 2017. https://doi.org/10.2172/1845414
18. Matlack KS, Muller IS, Abramowitz H, Joseph I, Pegg IL. Support for DF LAW flowsheet development (ORP-61653/VSL-17R4250-1). Washington, DC: Vitreous State Laboratory, The Catholic University of America; 2017. https://doi.org/10.2172/1420317
19. Matlack K, Pegg I. Estimates of acetonitrile generation from scale melter testing of LAW simulants (VSL-19S4573-1) (ORP-67600-00/VSL-19S4573-1, Rev A). Washington, DC: Vitreous State Laboratory, The Catholic University of America; 2019. https://doi.org/10.2172/1844981
20. Veach KJ. ETF acetonitrile steam stripper process control narrative. Sargent & Lundy for Washington River Protection Solutions, LLC. (RRP-RPT-62622). 2022.
21. Parsons. Waste treatment and immobilization plant high-level waste treatment analysis of alternatives (DE-NA0002895; Enterprise Construction Management Services). Richland, WA: Office of River Protection; 2023.
22. ,Brandys M, Mechlolsky N, Pegg IL. Acetonitrile destruction in ETF feed solutions by UV/OX and persulfate (WRPS-66058/VSL-20R4850-1). Richland, WA: Washington River Protection Solutions; 2020. https://doi.org/10.2172/1784544
23. Kunc J, Kloužek J, Vernerová M, Cincibusová P, Ferkl P, Hall MA, et al. Effect of feed composition on the production of off-gases during vitrification of simulated low-activity nuclear waste. Prog Nucl Energy. 2023;166:104932. https://doi.org/10.1016/j.pnucene.2023.104932
24. Lambert DP, Pickenheim BR, Stone ME, Newell JD, Best DR. Glycolic-formic acid flowsheet final report for downselection decision (SRNL-STI-2010-00523, 1013045). Jackson, SC: Savannah River National Laboratory; 2011. https://doi.org/10.2172/1013045
25. Larson DE. Hanford high-level waste vitrification program at the Pacific Northwest National Laboratory: technology development—annotated bibliography (PNNL-10955). Richland, WA: Pacific Northwest National Laboratory; 1996. https://doi.org/10.2172/394919
26. Smith PA, Vienna JD, Merz MD. NCAW feed chemistry: effect of starting chemistry on melter off-gas and iron redox (PNL-10517). Richland, WA: Pacific Northwest National Laboratory; 1995. https://doi.org/10.2172/211347
27. Rigby JC, Dixon DR, Kloužek J, Pokorný R, Thompson PBJ, Scrimshire A, et al. Alternative reductants for foam control during vitrification of high-iron high level waste (HLW) feeds. J Non-Cryst Solids. 2023;608:122240. https://doi.org/10.1016/j.jnoncrysol.2023.122240
28. Choi AS. Melter off-gas flammability assessment for DWPF alternate reductant flowsheet options (SRNL-STI-2011-00321; p. SRNL-STI-2011-00321, 1019027). Jackson, SC: Savannah River National Laboratory; 2011. https://doi.org/10.2172/1019027

29. Choi A. DWPF melter off-gas flammability model for the nitric-glycolic acid flowsheet (SRNL-STI-2014-00355). Jackson, SC: Savannah River National Laboratory; 2014. https://doi.org/10.2172/1154717
30. Han W-Q. Anisotropic hexagonal boron nitride nanomaterials: synthesis and applications (BNL-81439-2008-BC; Multi Metallic and Metal Oxide Nanomaterials for Life Sciences, pp. 1–60). New York: Center for Functional Nanomaterials, Brookhaven National Laboratory; 2010. https://doi.org/10.1002/9783527610419.ntls0161
31. Solozhenko VL, Turkevich VZ, Holzapfel WB. Refined phase diagram of boron nitride. J Phys Chem B. 1999;103(15):2903–5. https://doi.org/10.1021/jp984682c
32. Kostoglou N, Polychronopoulou K, Rebholz C. Thermal and chemical stability of hexagonal boron nitride (h-BN) nanoplatelets. Vacuum. 2015;112:42–45. https://doi.org/10.1016/j.vacuum.2014.11.009
33. Matlack KS, Abramowitz H, Muller IS, Joseph I, Pegg IL. DFLAW glass and feed qualifications for AP-107 to support WTP start-up and flow-sheet development (VSL-18R4500-1). Washington, DC: Vitreous State Laboratory, The Catholic University of America; 2018. https://doi.org/10.2172/1845088
34. Hilliard Z, Hrma P. A method for determining bulk density, material density, and porosity of melter feed during nuclear waste vitrification. J Am Ceram Soc. 2016;99(1):98–105. https://doi.org/10.1111/jace.13919
35. Marcial J, Luksic S, Kloužek J, Vernerová M, Cutforth D, Varga T, et al. In-situ X-ray and visual observation of foam morphology and behavior at the batch-melt interface during melting of simulated waste glass. Ceram Int. 2022;48(6):7975–85. https://doi.org/10.1016/j.ceramint.2021.11.344
36. McCloy J, Washton N, Gassman P, Marcial J, Weaver J, Kukkadapu R. Nepheline crystallization in boron-rich aluminosilicate glasses as investigated by multi-nuclear NMR, Raman, & Mössbauer spectroscopies. J Non-Cryst Solids. 2015;409:149–65. https://doi.org/10.1016/j.jnoncrysol.2014.11.013
37. Sutovich KJ, Peters AW, Rakiewicz EF, Wormsbecher RF, Mattingly SM, Mueller KT. Simultaneous quantification of Brønsted- and Lewis-acid sites in a USY zeolite. J Catal. 1999;183(1):155–58. https://doi.org/10.1006/jcat.1998.2379
38. Page JE, Topping CV, Scrimshire A, Bingham PA, Blundell SJ, Hayward MA. Doped Sr_2FeIrO_6—phase separation and a $J_{eff} \neq 0$ State for Ir^{5+}. Inorg Chem. 2018;57(16):10303–11. https://doi.org/10.1021/acs.inorgchem.8b01539
39. Ahmadzadeh M, Scrimshire A, Mottram L, Stennett MC, Hyatt NC, Bingham PA, et al. Structure of $NaFeSiO_4$, $NaFeSi_2O_6$, and $NaFeSi_3O_8$ glasses and glass-ceramics. Am Mineral. 2020;105(9):1375–84. https://doi.org/10.2138/am-2020-7285
40. Appel CJ, Kloužek J, Jani N, Lee SM, Dixon DR, Hrma P, et al. Effect of sucrose on foaming and melting behavior of a low-activity waste melter feed. J Am Ceram Soc. 2019;102(12):7594–605. https://doi.org/10.1111/jace.16675
41. Ferkl P, Hrma P, Abboud AW, Guillen DP, Vernerov M, Kloužek J, et al. Conversion degree and heat transfer in the cold cap and their effect on glass production rate in an electric melter. Int J Appl Glass Sci. 2023;14:318–29.
42. Khawand J, Kloužek J, Vernerová M, Cincibusová P, Hrma P, Kruger AA, et al. Effect of sucrose on the oxidation-reduction conditions and retention of rhenium during vitrification of low-activity waste. J Nucl Mater. 2023;573:154155. https://doi.org/10.1016/j.jnucmat.2022.154155
43. Marcial J, Pokorný R, Kloužek J, Vernerová M, Lee S, Hrma P, et al. Effect of water vapor and thermal history on nuclear waste feed conversion to glass. Int J Appl Glass Sci. 2020;12:145–57.
44. Gervais C, Maquet J, Babonneau F, Duriez C, Framery E, Vaultier M, et al. Chemically derived BN ceramics: extensive ^{11}B and ^{15}N solid-state NMR study of a preceramic polyborazilene. Chem Mater. 2001;13(5):1700–1707. https://doi.org/10.1021/cm001244l
45. Love AM, Thomas B, Specht SE, Hanrahan MP, Venegas JM, Burt SP, et al. Probing the transformation of boron nitride catalysts under oxidative dehydrogenation conditions. J Am Chem Soc. 2019;141(1):182–90. https://doi.org/10.1021/jacs.8b08165
46. Marcial J, Saleh M, Watson D, Martin SW, Crawford CL, McCloy JS. Boron-speciation and aluminosilicate crystallization in alkali boroaluminosilicate glasses along the $NaAl_{1-x}B_xSiO_4$ and $LiAl_{1-x}B_xSiO_4$ joins. J Non-Cryst Solids, 2019;506:58–67. https://doi.org/10.1016/j.jnoncrysol.2019.01.001
47. Darby Dyar M. A review of Mössbauer data on inorganic glasses: the effects of composition on iron valency and coordination. Am Miner. 1985;70(3–4):305–8.
48. Oh SJ, Cook DC, Townsend HE. Characterization of iron oxides commonly formed as corrosion products on steal. Hyperfine Interact. 1998;112:59–66.
49. Reigel MM. Literature review: assessment of DWPF melter and melter off-gas system lifetime. Jackson, SC: Savannah River National Laboratory; 2015. (SRNL-STI-2014-00134). https://doi.org/10.2172/1209042
50. Schreiber HD, Hockman AL. Redox chemistry in candidate glasses for nuclear waste immobilization. J Am Ceram Soc. 1987;70(8):591–94. https://doi.org/10.1111/j.1151-2916.1987.tb05712.x

SUPPORTING INFORMATION

Additional supporting information can be found online in the Supporting Information section at the end of this article.

How to cite this article: Rigby JC, Marcial J, Pokorny R, Kloužek J, Han KS, Washton N, et al. Boron nitride: Novel ceramic reductant for low-activity waste vitrification. J Am Ceram Soc. 2024;e20192. https://doi.org/10.1111/jace.20192